

# FedMed-ATL: Misaligned Unpaired Cross-Modality Neuroimage Synthesis via Affine Transform Loss

Jinbao Wang\*  
Southern University of Science and  
Technology  
Shenzhen, China  
linkingring@163.com

Guoyang Xie\*  
Southern University of Science and  
Technology  
Shenzhen, China  
University of Surrey  
Guildford GU2 7XH, UK  
xiegy2019@mail.sustech.edu.cn

Yawen Huang\*  
Tencent Jarvis Lab  
Shenzhen, China  
yawenhuang@tencent.com

Yefeng Zheng  
Tencent Jarvis Lab  
Shenzhen, China  
yefengzheng@tencent.com

Yaochu Jin  
Bielefeld University  
33619 Bielefeld, Germany  
University of Surrey  
Guildford GU2 7XH, UK  
yaochu.jin@surrey.ac.uk

Feng Zheng<sup>†</sup>  
CSE and RITAS, Southern University  
of Science and Technology  
Shenzhen, China  
f.zheng@ieee.org

## ABSTRACT

The existence of completely aligned and paired multi-modal neuroimaging data has proved its effectiveness in the diagnosis of brain diseases. However, collecting the full set of well-aligned and paired data is impractical, since the practical difficulties may include high cost, long time acquisition, image corruption, and privacy issues. Previously, the misaligned unpaired neuroimaging data (termed as MUD) are generally treated as noisy label. However, such a noisy label-based method fail to accomplish well when misaligned data occurs distortions severely. For example, the angle of rotation is different. In this paper, we propose a novel federated self-supervised learning (FedMed) for brain image synthesis. An affine transform loss (ATL) was formulated to make use of severely distorted images without violating privacy legislation for the hospital. We then introduce a new data augmentation procedure for self-supervised training and fed it into three auxiliary heads, namely auxiliary rotation, auxiliary translation and auxiliary scaling heads. The proposed method demonstrates the advanced performance in both the quality of our synthesized results under a severely misaligned and unpaired data setting, and better stability than other GAN-based algorithms. The proposed method also reduces the demand for deformable registration while encouraging to leverage the misaligned and unpaired data. Experimental results verify the outstanding performance of our learning paradigm compared to other state-of-the-art approaches.

\*Equally contribute to this work

Permission to make digital or hard copies of all or part of this work for personal or classroom use is granted without fee provided that copies are not made or distributed for profit or commercial advantage and that copies bear this notice and the full citation on the first page. Copyrights for components of this work owned by others than ACM must be honored. Abstracting with credit is permitted. To copy otherwise, or republish, to post on servers or to redistribute to lists, requires prior specific permission and/or a fee. Request permissions from [permissions@acm.org](mailto:permissions@acm.org).

MM '22, October 10–14, 2022, Lisboa, Portugal

© 2022 Association for Computing Machinery.

ACM ISBN 978-1-4503-9203-7/22/10...\$15.00

<https://doi.org/10.1145/3503161.3547762>

## CCS CONCEPTS

• **Computing methodologies** → **Computer vision tasks.**

## KEYWORDS

misaligned unpaired neuroimaging data, unsupervised learning, cross-modality neuroimage synthesis, federated learning

## ACM Reference Format:

Jinbao Wang, Guoyang Xie, Yawen Huang, Yefeng Zheng, Yaochu Jin, and Feng Zheng. 2022. FedMed-ATL: Misaligned Unpaired Cross-Modality Neuroimage Synthesis via Affine Transform Loss. In *Proceedings of the 30th ACM International Conference on Multimedia (MM '22)*, October 10–14, 2022, Lisboa, Portugal. ACM, New York, NY, USA, 10 pages. <https://doi.org/10.1145/3503161.3547762>

## 1 INTRODUCTION

The majority of existing medical datasets [2, 9, 43], especially for neuroimaging data, are high-dimensional and heterogeneous. For instance, positron emission tomography (PET) and magnetic resonance imaging (MRI) are the imaging techniques to measure the information of organs for auxiliary diagnosis or monitor treatment. The paired/registered multi-modal data provide the complementary information to investigate certain pathologies or neurodegenerations. However, it is often not feasible to acquire complete paired and aligned multi-modal neuroimaging data due to: 1) collecting multi-modal neuroimaging data is very costly; 2) many medical institutions cannot share their data, considering that medical data are especially restricted to the local regulations, despite the identifiable information can be removed for protecting the privacy of patients. 3) patients' motions may result in severe misaligned neuroimaging data. 4) state-of-the-art deformable registration algorithms require tens of minutes to hours for a pair of scans. Hence, most of neuroimaging data are dispersed into different hospitals with misaligned and unpaired property. To solve the above problem, we investigate such data in a realistic scenario. Specifically, we divide the misaligned phenomenon into three parts, severe rotation, severe translation and severe rescaling, which can be referred from

the second row of Figure 1. The misaligned data setting is similar to RegGAN [28], while we set more severe misalignment than that in RegGAN. In particular, the angle rotation setting, the translation setting and the rescaling setting in RegGAN are restricted in  $[-5, +5]$  degrees,  $[-25, +25]$  pixels and  $[0.9, 1.1]$  ratios, respectively. We set the angle rotation, the translation and the rescaling range in  $[-90, +90]$  degrees,  $[-30, +30]$  pixels, and  $[0.9, 1.2]$  ratios, respectively. The detailed simulation about the distribution settings of misaligned unpaired imaging data (MUD) can be referred to Section 4.

Deformable registration is a fundamental task for solving misaligned medical data. The purpose of deformable registration is to establish a dense and non-linear correspondence between a pair of images, such as 3D misaligned multi-modal neuroimaging data. Traditional methods [7, 27] align each voxel with a similar appearance by enforcing constraints on the registration mapping. Most of the traditional deformable registration methods can obtain high accuracy. However, they require very huge computation resources resulting in running slowly in practice. Guha et al. [10] adopt a CNN-based method to speed up the registration procedure. The work in [10] parameterizes the original deformable registration method as a CNN and optimizes the parameters of CNN by a set of paired but misaligned images. However, the doctors need to verify the effect of deformation algorithms by themselves. This approach inevitably results in a huge amount of labor work and long checking time. Therefore, the emerging issue is to effectively explore MUD rather than using deformable registration to facilitate brain image synthesis. Similar to FedMed-ATL, RegGAN [28] forms the misaligned images as the noisy label and utilizes the correction loss to minimize the error resulting from misalignment. However, the assumption of RegGAN [28] is that the neuroimaging data have slight distortions. In this case, RegGAN can convert the slight-distorted neuroimaging data as the noisy label. But in reality, some of the misaligned neuroimaging data inevitably meet with severe distortions. The proposed FedMed-ATL eliminates the requirements of RegGAN and treats MUD as the multi-view data augmentation for the discriminator training, which can significantly mitigate the mode collapse due to the side effect from MUD. Inspired by [13], FedMed-ATL reuses the discriminator as the encoder. More augmented views of MUD are generated by the Affine Transform Module, and then fed into the designed auxiliary heads, including auxiliary rotation head, auxiliary translation head and auxiliary rotation head. This action aims to strengthen the discriminator to distinguish the real and fake samples. We heuristically prove that FedMed-ATL outperforms RegGAN significantly in a severe distortion setting. Figure 2 provides detailed information.

Another issue for multi-modality brain image synthesis is data isolation and privacy concern. Although the collaborative research can be conducted by multiple hospitals, they may undertake integrated analysis rather than sharing research data with each other. Lately, a large amount of effort has been made to facilitate the availability of medical data without violating the privacy issue. Federated Learning (FL) is one of the popular approaches. FL is a decentralized approach where local clients train their local models without transmitting data to a central server, and the global model aggregates the gradients from clients [32]. In addition, FL with GANs has witnessed some pilot progress on image synthesis [5, 11, 44]. For example, DP-FedAvg-GAN [5] trains GANs with the

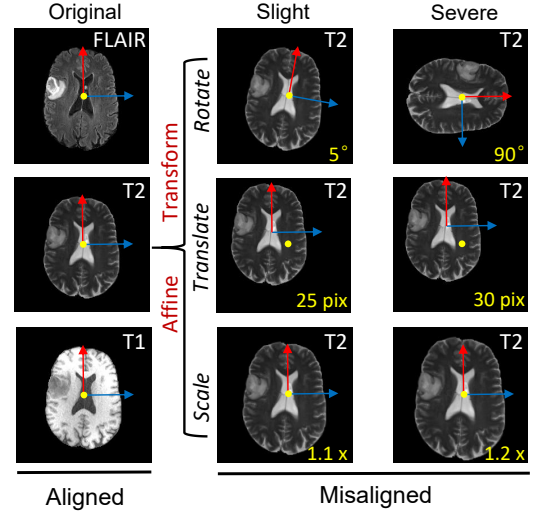


**Figure 1: Illustration of multi-modal images, including slightly and severely misaligned cases, paired and unpaired cases. Slight noise denotes the angle ranges in  $[-3^\circ, 3^\circ]$ , the translation ranges in  $[-15, +15]$  pixels and the scaling ratio ranges in  $[0.9, 1.1]$ . Severe noise denotes the angle ranges in  $[-90^\circ, 90^\circ]$ , the translation ranges in  $[-30, +30]$  pixels and the scaling ratio ranges in  $[0.9, 1.2]$ , respectively**

differential privacy-preserving algorithm, which clips the gradients to bound sensitivity and adds calibrated random noise to introduce stochasticity. FedMed-GAN [50] is similar to our work, however, they assume that all of the neuroimaging data are very clean, i.e., well-aligned in their experimental settings. FedMed-ATL assumes that all neuroimaging data from each hospital are MUD. We found that FedMed-ATL surpasses FedMed-GAN when each client's data is MUD. In addition, we also make a more comprehensive consideration in a realistic scenario and gives more assumptions for all possible data distribution settings and data misaligned conditions. For example, we assume that some hospitals' data are misaligned but paired, and the others are well aligned and paired. In other words, we need to consider both supervised and unsupervised GAN integrated into federated learning. In this case, we can find that the performance of FedMed-ATL is better than FedMed-GAN.

Our contributions can be summarized as follows:

- To the best of our knowledge, FedMed-ATL is the first algorithm to make use of the severely misaligned unpaired data (MUD) to facilitate the multi-modality brain image synthesis. FedMed-ATL reduces the demand for the deformable registration when neuroimaging data meet severe distortions.
- Inspired by self-supervised learning, FedMed-ATL treats MUD as a multi-view data augmentation procedure rather than noisy data. We propose three auxiliary losses to the discriminator, including auxiliary rotation, auxiliary translation and auxiliary rescaling losses (termed as the Affine Transform Loss). The proposed method shows good quality of the synthesized results under a severely misaligned

and unpaired data setting, and better stability than other Medical-GAN-based algorithms.

- FedMed-ATL encourages to realize the usage of those misaligned and unpaired data when compared with RegGAN, like 90° rotation and 20% translation. In addition, FedMed-ATL exceeds FedMed-RegGAN by a big margin when severe distortions occur in both misaligned and unpaired neuroimaging data.

## 2 RELATED WORK

### 2.1 Cross-Modality Medical Image Synthesis

The existing medical image-to-image translation [25, 28, 36] has demonstrated their considerable prospects for both research and clinical analysis. Of these methods, supervised GANs are still the mainstream for cross-modality neuroimaging data synthesis [16, 40, 49, 52, 53, 57]. However, synthesizing in a supervised manner requires paired data for training, which is difficult to implement in practice. To solve this problem, both semi-supervised and unsupervised methods are then launched to eliminate the need of paired data. Guo *et al.* [18] leverage a lesion segmentation network as a teacher to guide the generator by using unpaired training data. Shen *et al.* [42] and Zhou *et al.* [55] also utilize the high-level tasks to guide the cross-modality image synthesis. Huang *et al.* [21, 22] make fully use of unpaired cross-modality data and project them into a common space. The attributed features from the common space bring great helpful to synthesize the missing target modality data. Kong *et al.* [28] introduce a new I2IT model called RegGAN, which converts the unsupervised I2IT task into a supervised I2IT with noisy labels. However, RegGAN cannot deal with the severe distortion, which probably happens in the realistic scenarios.

### 2.2 Medical Image Deformable Registration

There is a lot of work for medical image registration, including statistical parametric mapping [4], elastic deformation model [8, 41], B-spline [39], Demons [35, 45] and discrete methods [15]. The work in [3] applies an image-to-image translation network to preserve the geometric property, which may be lost from deformable regularization. Recently, deep learning based methods are adapted to learn the parameters of deformation field. In total, deep learning based methods can be classified as supervised learning methods [17, 37] and unsupervised learning methods [31, 48]. The supervised learning methods require the ground truth deformation fields as the training dataset but the unsupervised methods do not need the ground truth. In addition, medical image registration methods can also be categorized as the displacement field [19, 51] and the diffeomorphic methods [14, 24, 34, 46]. The displacement methods can directly obtain the deformation field via CNN model. While the diffeomorphic methods desire to guarantee the diffeomorphic property by computing the diffeomorphic deformation field. Both of them aims to obtain better registration results instead of image synthesis. FedMed-ATL aims to utilize both misaligned and unpaired brain image data for synthesis without a registration procedure.

### 2.3 Federated Learning

Data isolation and privacy concerns are the fundamental problems which blocks a large-scale and multi-institute neuroimaging

research. Federated learning, as a privacy-preserving decentralization strategy, allows clients train their own models without data communication to a central server by aggregating client progresses to update a global model [29, 33, 47, 54]. FedAvg [33] combines local stochastic gradient descent (SGD) on each client with a server that performs model averaging. Yurochkin *et al.* [54] developed a Bayesian non-parametric framework for federated learning with neural networks. FedProx [29] provides a generalized and re-parametrized FedAvg that addresses the challenges of heterogeneity both theoretically and empirically. FedMA [47] constructs the shared global model in a layer-wise manner by matching and averaging hidden elements with similar feature extraction signatures. However, directly incorporating the generative adversarial framework into the federated learning is challenging, due to the cost functions may not converge using federated gradient aggregation in a min-max setting between the discriminator and the generator [6, 12, 44]. DP-FedAvg-GAN [6] provides a differential privacy-preserving algorithm, which clips the gradients to bound sensitivity and adds calibrated random noise to introduce stochasticity. GS-WGAN [12] enables the release of a sanitized version of sensitive data while maintaining stringent privacy protections. GS-WGAN is capable to distort gradient information, which allows to train a deeper model with more informative samples. Despite these methods demonstrate their reasonable results on different tasks, the performance on cross-modality image synthesis is untapped, let alone the theory or empirical explanations for the convergence. In addition, the proportion of paired and unpaired data for each client (hospital) and the long-tail data distribution problems are all neglected.

## 3 FEDMED-ATL

### 3.1 Federated Model Setup

The federated setting of our generator and discriminator is described in Figure 3. We employ CycleGAN [56] as our baseline model. CycleGAN [56] owns two generators  $G_{A \leftrightarrow B}$ , discriminators  $D_{A \leftrightarrow B}$ . Specifically,  $G_{A \rightarrow B}$  generates B-modal images from A-modal samples.  $D_{A \rightarrow B}$  distinguishes whether the generated B-modal data from A-modal sample is fake. The federated setting of CycleGAN is to locate two generators ( $G_{A \rightarrow B}$ ,  $G_{B \rightarrow A}$ ) into the servers. On the other hand, the generators are separately aggregated into the server's generators. Then, the server sends its generators into different hospitals. The discriminators ( $D_{A \rightarrow B}$ ,  $D_{B \rightarrow A}$ ) of each client are independent.

### 3.2 Misaligned Unpaired Data Distribution

We address the task of federated self-supervised learning for MUD by formulating several realistic settings. To simulate the real data distribution as much as possible, we adopt the following settings as shown in Figure 4.

Firstly, we divide ready-made data into several clients, where each client has its own private and unique data. Meanwhile, these clients (hospitals) contain unbalanced multi-modal images, i.e. having different numbers of patients in each client or having different numbers of images in each modality. Secondly, without losing generality, we explore both paired and unpaired cases in our experiments. For example, we randomly select the multi-modal slices from the

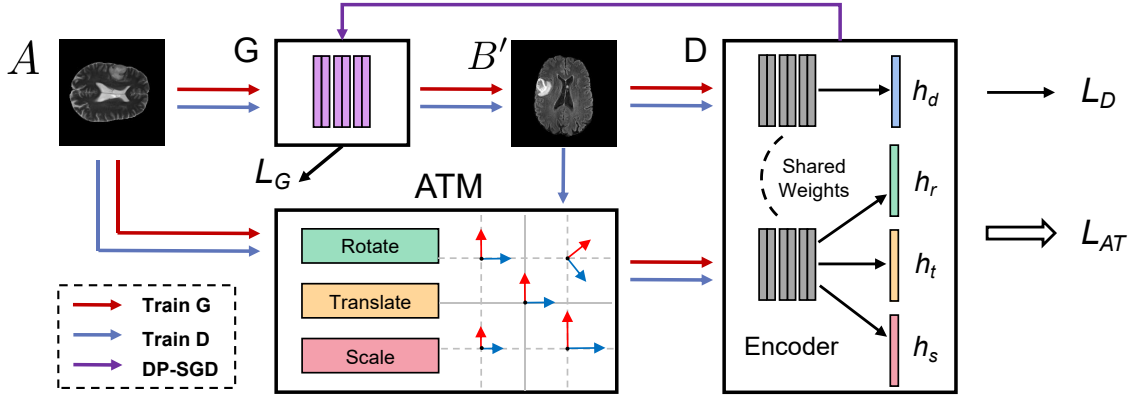


**Figure 2: The pipeline of FedMed-ATL.** The generator  $G$  generates B-modal images  $B'$  from A-modal. The discriminator  $D$  distinguishes  $B'$  from real or fake. The affine transform module (ATM) achieves image transform. The functions of  $L_G$ ,  $L_D$ , and  $L_{AT}$  are the generator loss, the discriminator loss, and the affine transform loss, respectively. To train  $G$  and  $D$ , the red line and blue line describe the data flow. Note that input A-model images are fed into  $G$  and ATM for training  $G$ , but both input A-model images and generated B-model images  $B'$  are fed into  $D$ . In ATM, three transform blocks (Rotate, Translate, Scale) provide a rich data resource. For federated learning, we add DP-SGD [1] (purple line) to avoid privacy leakage.

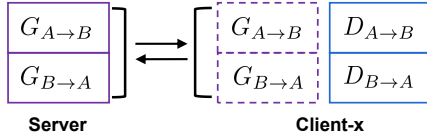


**Figure 3: The federated setting of FedMed-ATL model.**  $G$  denotes the shared generator and  $D$  denotes the discriminator. The discriminator of each client does not participate into the aggregation process. Only the generator of each client join into the aggregation process.

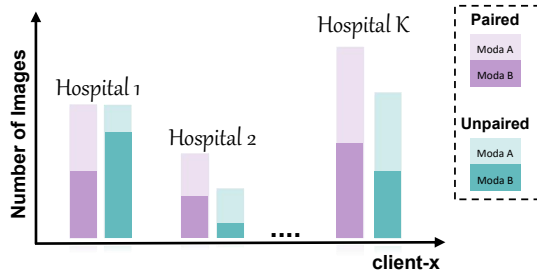


**Figure 4: Distribution of misaligned unpaired data (MUD).** For instance, Hospital 1 has paired data with misaligned attributes, while Hospitals of 2-K have MUD in the most real-life case.

same patient as paired data like in Hospital 1 or select them from patients with different IDs as unpaired data like in Hospital 2. After that, we randomly transform the input images at a certain threshold of rotation, translation and scaling, and there is the majority of misaligned images in the constructed training set.

### 3.3 Network Architectures

**Generator** In general, the architecture of generator could be encoder-decoder style. The performance of FedMed-ATL is not being affected by the specific generator's architecture. In Figure 2, FedMed-ATL use U-Net [38] as the generator.

**Discriminator** Inspired by Chen *et.al.* [13], FedMed-ATL reuses the original discriminator as the encoder. The architecture of discriminator is similar to CycleGAN [56], MUNIT [20] and UNIT [30] except the last layer. FedMed-ATL replaces the last layer of the discriminator with a two-layer MLP (termed as discriminator head). In Figure 2,  $h_d$  represents the discriminator head. The input and output dimensions of two layers are (512, 128) and (128, 1), respectively. The role of the discriminator head is to distinguish the real or fake samples.

**Affine Transform Module (ATM)** ATM contains three operators, namely rotation, translation and rescaling. As for rotations, the rotation degree is chosen in  $[0^\circ, 90^\circ, 180^\circ, 270^\circ]$ . As for translation, the x-axis and y-axis translation is chosen in  $[(-30, -30), (-30, 30), (30, -30), (30, 30)]$ . As for rescaling, the scaling ratio is chosen in  $[0.9, 1.1, 1.2]$ . We conduct a comprehensive ablation study on the number of views for each operation. The number of views is a range in  $[1, 2, 4]$ . For instance, if the number of views is 4, FedMed-ATL picks 4 augmented image data from rotation, translation and rescaling, and then feeds them into auxiliary rotation head, auxiliary translation head and auxiliary rescaling head, respectively. In addition, when FedMed-ATL trains the generators, only the real samples are fed into ATM. The real and fake samples are fed into the ATM during the discriminator training procedure. This treatment encourages the generator to induce more 'really misaligned' samples for the discriminator to avoid overfitting.

**Auxiliary Rotation Head** The role of auxiliary rotation head ( $h_r$  in Figure 2) is to distinguish the rotation angle of the neuroimaging data, i.e.,  $0^\circ, 90^\circ, 180^\circ$  and  $270^\circ$ . Before going into the auxiliary

rotation head, FedMed-ATL needs to feed them into the encoder. This encoder is shared with the other heads, including the discriminator head, translation head, and scaling head. In Equation 1,  $x$  are the real samples when FedMed-ATL update the parameters of generators. In Equation 1,  $x$  denotes both the real sample and fake samples (the generated samples) when FedMed-ATL updates the parameters of discriminators.  $P_{h_r}(R|x^r)$  is the predictive distribution of auxiliary rotation head over the angles of rotation of the sample. The intuition of auxiliary rotation loss is to enable the discriminator to access more severe rotated samples. Since the rotation head and discriminator head share the same encoder, i.e., these two heads own similar features. In this case, even if the discriminator meets with the severely rotated samples, the auxiliary rotation loss can help the discriminator to distinguish real or fake samples without being affected by severe rotation.

**Auxiliary Translation Head** The role of auxiliary translation head ( $h_t$  in Figure 2) is to distinguish the translation distance of the neuroimaging data, i.e.  $[(-30, -30), (-30, 30), (30, -30), (30, 30)]$ . Similarly,  $x$  denotes the real sample when FedMed-ATL updates the parameters of generators.  $P_{h_t}(T|x^t)$  is the predictive distribution of auxiliary translation head over the translation direction and distance of the sample. The aim of auxiliary translation loss is similar to the auxiliary rotation loss. In this case, the discriminator is able to access more severe translated samples. The auxiliary translation loss can support the discriminator to distinguish real or fake samples without being affected by severe translation.

**Auxiliary Rescaling Head** The role of auxiliary rescaling head ( $h_s$  in Figure 2) is to distinguish the rescaling ratio of neuroimaging data, i.e.  $[0.9, 1.1, 1.2]$ . Similar to the above two heads,  $P_{h_s}(S|x^s)$  denotes the predictive distribution of auxiliary rescaling head over the scaling ratio of the sample. The auxiliary scaling loss can further help the discriminator to distinguish the synthesized samples without being affected by severe rescaling.

### 3.4 Loss Function

**AT Loss** Three affine transform modes, namely rotation, translation, and scaling, are defined as follows.

$$L_{rot} = \lambda_{rot} \cdot \mathbb{E}[\log P_{h_r}(R = r|x^r)] \quad (1)$$

$$L_{trans} = \lambda_{trans} \cdot \mathbb{E}[\log P_{h_t}(T = t|x^t)] \quad (2)$$

$$L_{scale} = \lambda_{scale} \cdot \mathbb{E}[\log P_{h_s}(S = s|x^s)] \quad (3)$$

**GAN and Cycle Loss** Equation (4) is the loss function of GAN [23], where  $G$  is the generator that generates B-modal images from A-modal images, and  $D$  is the discriminator that distinguishes whether B-modal images generated from A-modal samples is fake.

$$\min_G \max_G L_{adv}(G, D) = \mathbb{E}_y [\log(D(y))] + \mathbb{E}_x [\log(1 - D(G(x)))] \quad (4)$$

Equation (5) is Cycle loss function [56], where  $F$  is the generator that generate A-modal image from B-modal images.

$$\min_G \max_G L_{cyc}(G, F) = \mathbb{E}_x [||F(G(x)) - x||_1] + \mathbb{E}_y [||G(F(y)) - y||_1] \quad (5)$$

**Total Loss** Overall, the total loss function is defined as:

$$L_{total} = \lambda_{rot} \cdot L_{rot} + \lambda_{trans} \cdot L_{trans} + \lambda_{scale} \cdot L_{scale} + \lambda_{adv} \cdot L_{adv} + \lambda_{cyc} \cdot L_{cyc}. \quad (6)$$

The weight  $\lambda$  of various loss functions will be introduced in the implementation part of Section 4.

## 4 EXPERIMENT

### 4.1 Federated Settings

**IXI** [2] collects nearly 600 MR images from normal and healthy subjects at three hospitals. The MR image acquisition protocol for each subject includes T1, T2, PD-weighted images (PD), MRA images, and Diffusion-weighted images. In this paper, we only use T1 (581 cases), T2 (578 cases) and PD (578 cases) data to conduct our experiments, and select the paired data with the same ID from the three modes. The image has a non-uniform length on the z-axis with the size of 256 on the x-axis and y-axis. The IXI dataset is not divided into a training set and a test set. Therefore, we randomly split the whole data as the training set (80%) and the test set (20%).

**BraTS2021** [9, 43] is constructed for analysis and diagnosis of brain disease. The publicly available dataset of multi-institutional and pre-operative MRI sequences is provided, which includes both training data (1251 cases) and validation data (219 cases). Each 3D volume has 155×240×240 size imaged by four sequences: T1, T2, T1ce, and FLAIR.

**Data processing** To ensure data validity and diversity, we remove a skull without tissues in a slice, and split the three-dimensional volume and select slices from 50 to 80 on the Z-axis. All of the images in all datasets are cropped into the size of 256 pixels. We define unpaired data as two modal slices (T1, FLAIR) from two volumes (A and B) with the same N-th slice, e.g., unpaired data [T1-A-N, FLAIR-B-N]. By affinely transforming  $at(\cdot)$  both two modal images, we obtain a MUD-liked data [ $at(T1-A-N)$ ,  $at(FLAIR-B-N)$ ]. In our federated scenario, we first divide the training data (volume) proportionally into 4 clients based on the size of client data [0.4, 0.3, 0.2, 0.1], where each client has its own private and unique ones. After that, we construct MUDs in each client via the generation principle of unpaired data and misaligned data. In the training stage, we select overall 6,000 images from the IXI and BraTS2021 datasets, and each client selects 2,400, 1,800, 1,200, and 600 from the corresponding dataset. For evaluation, we use 3,462 images as our validation data from the IXI dataset, and 6,570 images from the BraTS2021 dataset, respectively.

**Metrics** We employ three metrics to evaluate our generator's performance. The first is mean absolute error (MAE):

$$MAE = \frac{1}{nm} \sum_n \sum_m^{j=1} |T_{ij} - G_{ij}|, \quad (7)$$

where  $T_{ij}$  denotes the ground truth neuroimage pixel and  $G_{ij}$  denotes the generated neuroimage pixel. The lower value of MAE means the better performance.

The second metric is the peak signal-to-noise ratio (PSNR). PSNR is a function of the mean squared error and better to evaluate the context (edge) detail of neuroimages. The higher PSNR value means

**Table 1: Comparison results of modal generation (from PD to T2) on the IXI dataset.**

Method	Slight Noise			Severe Noise		
	MAE ↓	PSNR ↑	SSIM ↑	MAE ↓	PSNR ↑	SSIM ↑
FedMed-C (+reggan)	0.0294	<b>26.0068</b>	<b>0.9614</b>	0.0302	24.5915	0.9477
FedMed-C	0.0385	24.9238	0.9545	0.0295	<b>25.0715</b>	<b>0.9555</b>
FedMed-C-ATL	<b>0.0279</b>	25.0844	0.9560	<b>0.0290</b>	24.7132	0.9517

**Table 2: Comparison results of modal generation (from T1 to FLAIR) on the BraTS2021 dataset.**

Method	Slight Noise			Severe Noise		
	MAE ↓	PSNR ↑	SSIM ↑	MAE ↓	PSNR ↑	SSIM ↑
FedMed-C (+reggan)	0.0481	19.8538	0.8841	0.0455	20.0179	0.8950
FedMed-C	0.0466	20.0601	0.9003	0.0474	19.9319	0.8928
FedMed-C-ATL	<b>0.0447</b>	<b>20.3961</b>	<b>0.9044</b>	<b>0.0439</b>	<b>20.8232</b>	<b>0.9123</b>

the better performance.

$$PSNR = -10 \log_{10} \left( \frac{1}{nm} \sum_n \sum_m (T_{ij} - G_{ij})^2 \right) \quad (8)$$

The third metric is structural similarity index (SSIM), which is a weighted combination of the luminance, the contrast and the structure. The higher SSIM value means the better performance.

$$SSIM = \frac{(2\mu_T\mu_G + C_1)(2\sigma_{TG} + C_2)}{(\mu_T^2 + \mu_G^2 + C_1)(\sigma_T^2 + \sigma_G^2 + C_2)} \quad (9)$$

The  $\mu$  and  $\sigma$  in SSIM are the mean value and standard deviation of an image, respectively.  $C_1$  and  $C_2$  are two positive constants. We set  $C_1$  and  $C_2$  are 0.01 and 0.03, respectively. The values with lower MAE, the higher PSNR and SSIM denote the higher quality of the synthesized images.

**Implementations** In the federated scenario, there are 4 clients in our experiment, where the number of volumes owned by each client is 0.4 0.3, 0.2 and 0.1 respectively. We run 3 rounds for federated training, and each client is trained for 3 epochs. The model aggregation strategy is based on Fed-Avg [32], which aggregates the weight from each client’s generator model to the server model according to the data proportion distribution for each client. Specifically, we use the learning rate of  $1e-4$ , and the batch size of 4. The optimizer is Adam [26]. Its beta1 and beta2 are 0.5 and 0.999, respectively. The weights of GAN loss  $\lambda_{adv}$  and Cycle loss  $\lambda_{cyc}$  are 1.0, 10.0, respectively. For the affine transform loss (ATL), we set weights of rotation  $\lambda_{rot}$ , translation  $\lambda_{trans}$  and scaling  $\lambda_{scale}$  to 1.0 for each model’s generator and 0.5 for its discriminator, respectively. In FedMed-ATL differential privacy settings, the level of gradient clip bound, sensitivity, and noise multiplier is fixed to 1.0, 2.0, and 1.07, respectively. In terms of differential privacy setting, the Gaussian noise  $\mu$  is set to 1.07, and the standard deviation  $\sigma$  is set to 2.0. The clip bound for the back-propagation gradient is 1.0.

**Slight and Severe Noise** In our experiments, slight noise denotes the noise level is 3 like RegGAN [28]. Specifically, slight noise denotes the angle ranges in  $[-3^\circ, 3^\circ]$ , the translation ranges in  $[-15, +15]$  pixels and the scaling ratio ranges in  $[0.9, 1.1]$ . On the other hand, severe noise denotes the angle ranges in  $[-90^\circ, 90^\circ]$ , the translation ranges in  $[-30, +30]$  pixels and the scaling ratio ranges in  $[0.9, 1.2]$ , respectively.

## 4.2 Main Results

For the notation used in Table 1, Table 2, Table 3 and Table 4, M, C and U are the short names for MUNIT [20], CycleGAN [56] and UNIT [30], respectively.

**FedMed-C** denotes that we only put CycleGAN into our federated settings, which was introduced in Section 3.1 and Section 4.1 by adopting cycle loss (5) and adversarial loss (4). **FedMed-C (+reggan)** denotes that FedMed-C adopts the correction loss and registration network described in RegGAN [28]. **FedMed-C-ATL** denotes that FedMed-C employs the affine transform loss (ATL), which was introduced in Equation (6).

Table 1 and Table 3 show the results of the generated T2 from PD in the IXI dataset. Table 2 and Table 4 show the results of the generated FLAIR from T1 in the BraTS2021 dataset.

## 4.3 Ablation Study

**Analysis of ATL** To evaluate the performance of the affine transform loss, we test rotation, translation and scaling, respectively. **FedMed-C-AR** denotes that FedMed-C just employs the auxiliary rotation loss shown in Equation (1). **FedMed-C-AT** denotes that FedMed-C just employs the auxiliary translation loss given in Equation (2). **FedMed-C-AS** denotes that FedMed-C just employs the auxiliary scaling loss provided in Equation (3).

**Analysis of Different Views in ATL** We further investigate the impact of different views on ATL. **FedMed-C-ATL-1View** denotes that FedMed-C-ATL randomly picks one augmented view from the ATM Module and feeds it into the encoder (discriminator), which is described in Figure 2 and Section 3.3. In other words, there is only one augmented view to feed into the auxiliary rotation head, auxiliary translation head, and auxiliary rescaling head, respectively. **FedMed-C-ATL-2Views** denotes that FedMed-C-ATL randomly picks two augmented views and feeds them into the encoder (discriminator). The specific operation is similar to FedMed-C-ATL-1View, while the number of views is 2. **FedMed-C-ATL-4Views** denotes that FedMed-C-ATL picks four augmented views and feeds them into the encoder (discriminator). Note that in the previous description, the default way is to pick 4 views if this paper does not mention the number of views explicitly.

**Key Findings 1** We compare FedMed-C-ATL with the existing state-of-the-art algorithm, i.e. RegGAN [28]. We can observe that

**Table 3: Results of modal generation (from PD to T2) on the IXI dataset.**

Method	Slight Noise			Severe Noise		
	MAE ↓	PSNR ↑	SSIM ↑	MAE ↓	PSNR ↑	SSIM ↑
FedMed-C	0.0385	24.9238	0.9545	0.0295	<b>25.0715</b>	<b>0.9555</b>
FedMed-C-AR	<b>0.0261</b>	<b>25.3358</b>	<b>0.9577</b>	0.0298	24.3385	0.9467
FedMed-C-AT	0.0271	25.2926	0.9569	0.0291	24.7600	0.9509
FedMed-C-AS	0.0297	24.7426	0.9508	0.0316	24.0586	0.9410
FedMed-C-ATL-1View	0.0311	24.7486	0.9562	0.0331	24.2766	0.9518
FedMed-C-ATL-2Views	0.0288	24.8814	0.9562	0.0305	24.3427	0.9488
FedMed-C-ATL-4Views	0.0279	25.0844	0.9560	<b>0.0290</b>	24.7132	0.9517

**Table 4: Results of modal generation (from T1 to FLAIR) on the BraTS2021 dataset.**

Method	Slight Noise			Severe Noise		
	MAE ↓	PSNR ↑	SSIM ↑	MAE ↓	PSNR ↑	SSIM ↑
FedMed-C	0.0466	20.0601	0.9003	0.0474	19.9319	0.8928
FedMed-C-AR	0.0483	19.9217	0.8904	0.0439	20.4555	0.9056
FedMed-C-AT	0.0466	20.2059	0.8944	0.0440	20.4512	0.9042
FedMed-C-AS	0.0459	20.0981	0.8956	<b>0.0435</b>	20.6446	0.9093
FedMed-C-ATL-1View	0.0451	<b>20.6151</b>	<b>0.9085</b>	0.0439	20.8199	0.9115
FedMed-C-ATL-2Views	0.0451	20.2883	0.9012	0.0459	20.4236	0.9047
FedMed-C-ATL-4Views	<b>0.0447</b>	20.3961	0.9044	0.0439	<b>20.8232</b>	<b>0.9123</b>

FedMed-C-ATL outperforms FedMed-RegGAN by a large margin in a severe MUD setting, which achieves 2.4 % - 4.6 % absolute improvements in MAE, PSNR and SSIM, respectively. The results demonstrate that FedMed-C-ATL has a better ability to facilitate the quality of the synthesis, even if the input data suffered from a severe distortion. In addition, FedMed-C-ATL achieves absolute improvements of 10 %, 2.7 % and 2.7 % in slight MUD setting, when compared with FedMed+RegGAN. The improvement demonstrates the effectiveness of our FedMed-C-ATL for the slight MUD scenario. We also observe that FedMed-C performs slightly better than FedMed-C-ATL in the severe MUD settings on the IXI dataset. The principal reason is that data augmentation of FedMed-C-ATL results in opposite effect, when facing a very clean dataset like IXI. Here, “clean” does not mean a well-aligned and paired dataset, instead, it means healthy subject. From the results, we found that excessive data augmentations for a clean dataset are meaningless and even harmful for synthesis.

**Key Findings 2** To further evaluate the effectiveness of FedMed-C-ATL, we provide an ablation study to verify the usefulness of various auxiliary heads. In Table 4, the results show that by adding more heads can improve performance in a severe MUD setting. Specifically, FedMed-C-ATL-4views outperforms FedMed-C-AS by a large margin in a severe MUD setting, which achieves 6.8 %, 1.7 % and 1.1 % absolute improvements in MAE, PSNR and SSIM, respectively. From Table 3, FedMed-C-ATL-4views surpasses FedMed-C-AS by 1.1 % and 2.1 % in MAE, PSNR and SSIM, respectively.

**Key Findings 3** Furthermore, we desire to understand what quantity is suitable for data augmentation. From Table 4 and Table 3, we observe that FedMed-C-ATL-4views outperforms FedMed-C-ATL-1view and FedMed-C-ATL-2views in severe MUD settings. For example, FedMed-C-ATL-4views outperforms FedMed-C-ATL-1view by 1.2 %, 2.1 % and 2.7 % in MAE, PSNR and SSIM, respectively.

It demonstrates that the number of data augmentation plays a positive role in the quality of the synthesized results, especially in severe MUD settings.

#### 4.4 Visualization

To present the performance of the synthesized images by our federated mode (FedMed), we provide the generated results of FedMed-C (+reggan) and FedMed-C-ATL in IXI (Figure 5) and BraTS (Figure 6), the generated results of FedMed-C-ATL-1view, FedMed-C-ATL-2views, FedMed-C-ATL-4views in Figure 7 and the generated results of FedMed-C-AR, FedMed-C-AT, FedMed-C-AS and FedMed-C-ATL in Figure 8. From the results, we can see that FedMed-C-ATL has the ability to generate high-quality images, where the texture information of tissues and modal style would be well maintained.

## 5 CONCLUSIONS

In practice, the misaligned and unpaired neuroimaging data (MUD) are inevitable, however, the traditional deformable registration methods require expensive computational resources. From our perspectives, MUD can be regarded as data augmentation, and can be treated as an important manner to improve the quality of the synthesized neuroimaging data. FedMed-ATL provides a simple but effective way to facilitate multi-modal brain image synthesis. We prove that FedMed-ATL outperforms state-of-the-art algorithm when data in severe MUD settings. Hopefully, FedMed-ATL can motivate the medical GAN community to focus on the severe MUD scenario.

## 6 ACKNOWLEDGMENTS

This work is supported by the National Natural Science Foundation of China under Grant No. 61972188 and 62122035.



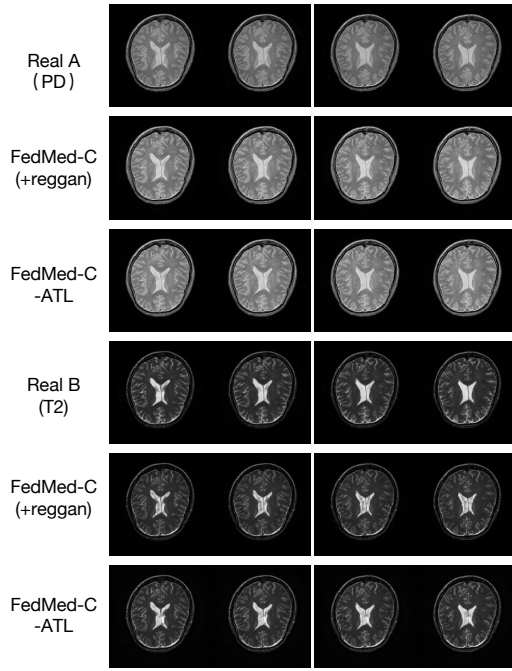


**Figure 5: Visualization of brain images generated by FedMed-C (+reggan) and FedMed-C-ATL on the IXI validation set. The model is trained on the severe noise scheme. The row images represent two volume examples of two near slices.**

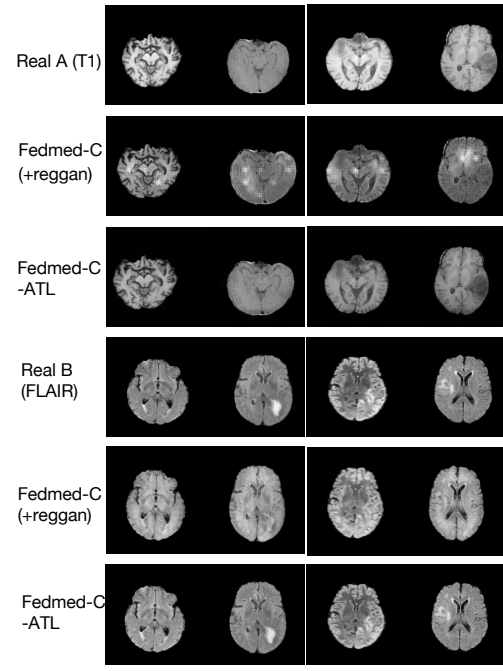


**Figure 6: Visualization of brain images generated by FedMed-C (+reggan) and FedMed-C-ATL on the BraTS validation set. The model is trained on the severe noise scheme. The row images represent two volume examples of two near slices.**

## REFERENCES

- [1] Martin Abadi, Andy Chu, Ian Goodfellow, H Brendan McMahan, Ilya Mironov, Kunal Talwar, and Li Zhang. 2016. Deep learning with differential privacy. In *Proceedings of the 2016 ACM SIGSAC conference on computer and communications security*. 308–318.
- [2] Paul Aljabar, Robin Wolz, Latha Srinivasan, Serena J. Counsell, Mary A. Rutherford, Anthony David Edwards, Joseph V. Hajnal, and Daniel Rueckert. 2011. A Combined Manifold Learning Analysis of Shape and Appearance to Characterize Neonatal Brain Development. *IEEE Transactions on Medical Imaging* 30 (2011), 2072–2086.
- [3] Moab Arar, Yiftach Ginger, Dov Danon, Amit H Bermanto, and Daniel Cohen-Or. 2020. Unsupervised multi-modal image registration via geometry preserving image-to-image translation. In *Proceedings of the IEEE/CVF conference on computer vision and pattern recognition*. 13410–13419.
- [4] John Ashburner and Karl J Friston. 2000. Voxel-based morphometry—the methods. *Neuroimage* 11, 6 (2000), 805–821.
- [5] Sean Augenstein, H Brendan McMahan, Daniel Ramage, Swaroop Ramaswamy, Peter Kairouz, Mingqing Chen, Rajiv Mathews, et al. 2019. Generative models for effective ML on private, decentralized datasets. *arXiv preprint arXiv:1911.06679* (2019).
- [6] Sean Augenstein, H. Brendan McMahan, Daniel Ramage, Swaroop Ramaswamy, Peter Kairouz, Mingqing Chen, Rajiv Mathews, and Blaise Agüera y Arcas. 2020. Generative Models for Effective ML on Private, Decentralized Datasets. In *ICLR*. OpenReview.net.
- [7] Brian B Avants, Nicholas J Tustison, Gang Song, Philip A Cook, Arno Klein, and James C Gee. 2011. A reproducible evaluation of ANTs similarity metric performance in brain image registration. *Neuroimage* 54, 3 (2011), 2033–2044.
- [8] Ruzena Bajcsy and Stane Kovačič. 1989. Multiresolution elastic matching. *Computer vision, graphics, and image processing* 46, 1 (1989), 1–21.
- [9] Spyridon Bakas, Hugo J. Kuijff, Bjoern H. Menze, and Mauricio Reyes. 2017. Brainlesion: Glioma, Multiple Sclerosis, Stroke and Traumatic Brain Injuries. In *Lecture Notes in Computer Science*.
- [10] Guha Balakrishnan, Amy Zhao, Mert R Sabuncu, John Guttag, and Adrian V Dalca. 2019. Voxelmorph: a learning framework for deformable medical image registration. *IEEE transactions on medical imaging* 38, 8 (2019), 1788–1800.

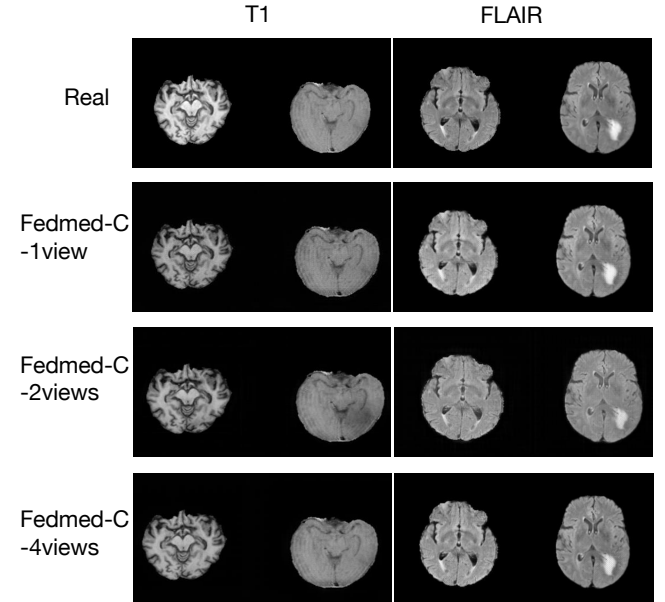


**Figure 7: Visualization of brain images generated by FedMed-C-ATL-1view, FedMed-C-ATL-2views and FedMed-C-ATL-4Views on the BraTS validation set. The model is trained on the severe noise scheme.**



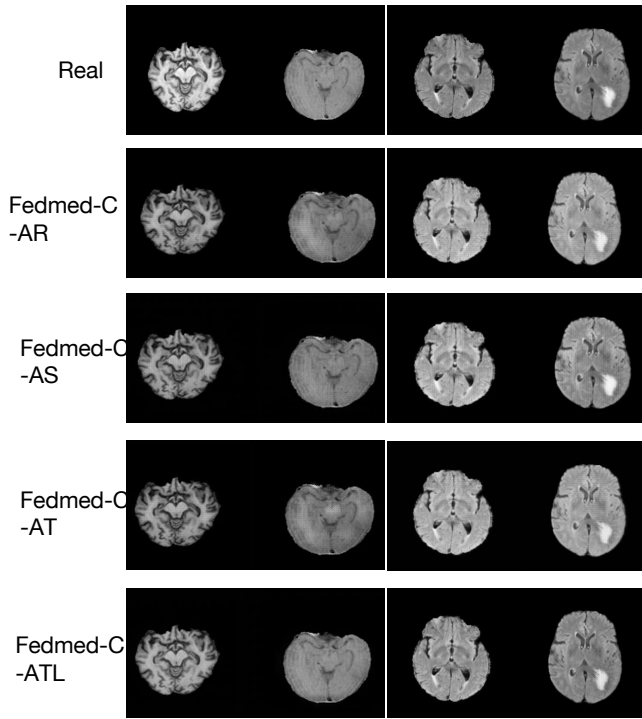


**Figure 8: Visualization of brain images generated by FedMed-C-AR, FedMed-C-AT, FedMed-C-AS and FedMed-C-ATL on the BraTS validation set. The model is trained on the severe noise scheme.**

- [11] Dingfan Chen, Tribhuvanesh Orekondy, and Mario Fritz. 2020. Gs-wgan: A gradient-sanitized approach for learning differentially private generators. *arXiv preprint arXiv:2006.08265* (2020).
- [12] Dingfan Chen, Tribhuvanesh Orekondy, and Mario Fritz. 2020. GS-WGAN: A Gradient-Sanitized Approach for Learning Differentially Private Generators. In *NeurIPS*.
- [13] Runfa Chen, Wenbing Huang, Binghui Huang, Fuchun Sun, and Bin Fang. 2020. Reusing discriminators for encoding: Towards unsupervised image-to-image translation. In *Proceedings of the IEEE/CVF Conference on Computer Vision and Pattern Recognition*. 8168–8177.
- [14] Adrian V. Dalca, Guha Balakrishnan, John V. Guttag, and Mert Rory Sabuncu. 2019. Unsupervised Learning of Probabilistic Diffeomorphic Registration for Images and Surfaces. *Medical image analysis* 57 (2019), 226–236.
- [15] Adrian V Dalca, Andreea Bobu, Natalia S Rost, and Polina Golland. 2016. Patch-based discrete registration of clinical brain images. In *International Workshop on Patch-based Techniques in Medical Imaging*. Springer, 60–67.
- [16] Salman Ul Hassan Dar, Mahmut Yurt, Levent Karacan, Aykut Erdem, Erkut Erdem, and Tolga Çukur. 2019. Image Synthesis in Multi-Contrast MRI With Conditional Generative Adversarial Networks. *IEEE Transactions on Medical Imaging* 38 (2019), 2375–2388.
- [17] Jingfan Fan, Xiaohuan Cao, Zhong Xue, Pew-Thian Yap, and Dinggang Shen. 2018. Adversarial Similarity Network for Evaluating Image Alignment in Deep Learning Based Registration. *Medical image computing and computer-assisted intervention : MICCAI ... International Conference on Medical Image Computing and Computer-Assisted Intervention* 11070 (2018), 739–746.
- [18] Pengfei Guo, Puyang Wang, Rajeev Yasarla, Jinyuan Zhou, Vishal M. Patel, and Shanshan Jiang. 2021. Anatomic and Molecular MR Image Synthesis Using Confidence Guided CNNs. *IEEE Transactions on Medical Imaging* 40 (2021), 2832–2844.
- [19] Mattias P. Heinrich and Lasse Hansen. 2020. Highly Accurate and Memory Efficient Unsupervised Learning-Based Discrete CT Registration Using 2.5D Displacement Search. In *MICCAI*.
- [20] Xun Huang, Ming-Yu Liu, Serge J. Belongie, and Jan Kautz. 2018. Multimodal Unsupervised Image-to-Image Translation. In *ECCV (3) (Lecture Notes in Computer Science, Vol. 11207)*. Springer, 179–196.
- [21] Yawen Huang, Feng Zheng, Runmin Cong, Weilin Huang, Matthew R. Scott, and Ling Shao. 2020. MCMT-GAN: Multi-Task Coherent Modality Transferable GAN for 3D Brain Image Synthesis. *IEEE Transactions on Image Processing* 29 (2020), 8187–8198.
- [22] Yawen Huang, Feng Zheng, Danyang Wang, Junyu Jiang, Xiaoqian Wang, and Ling Shao. 2020. Super-Resolution and Inpainting with Degraded and Upgraded Generative Adversarial Networks. In *IJCAI*.
- [23] Phillip Isola, Jun-Yan Zhu, Tinghui Zhou, and Alexei A. Efros. 2017. Image-to-Image Translation with Conditional Adversarial Networks. In *CVPR*. IEEE Computer Society, 5967–5976.
- [24] Xi Jia, Alexander Thorley, Wei Chen, Huaqi Qiu, Linlin Shen, Iain B. Styles, Hyung Jin Chang, Ale Leonardis, Antonio de Marvao, Declan P. O'Regan, Daniel Rueckert, and Jinming Duan. 2022. Learning a Model-Driven Variational Network for Deformable Image Registration. *IEEE Transactions on Medical Imaging* 41 (2022), 199–212.
- [25] Gongfa Jiang, Yao Lu, Jun Wei, and Yuesheng Xu. 2019. Synthesize mammogram from digital breast tomosynthesis with gradient guided cGANs. In *International Conference on Medical Image Computing and Computer-Assisted Intervention*. Springer, 801–809.
- [26] Diederik P Kingma and Jimmy Ba. 2014. Adam: A method for stochastic optimization. *arXiv preprint arXiv:1412.6980* (2014).
- [27] Arno Klein, Jesper Andersson, Babak A Ardekani, John Ashburner, Brian Avants, Ming-Chang Chiang, Gary E Christensen, D Louis Collins, James Gee, Pierre Hellier, et al. 2009. Evaluation of 14 nonlinear deformation algorithms applied to human brain MRI registration. *Neuroimage* 46, 3 (2009), 786–802.
- [28] Lingke Kong, Chenyu Lian, Detian Huang, Zhenjiang Li, Yanle Hu, and Qichao Zhou. 2021. Breaking the Dilemma of Medical Image-to-image Translation. *arXiv:2110.06465 [eess.IV]*
- [29] Tian Li, Anit Kumar Sahu, Manzil Zaheer, Maziar Sanjabi, Ameet Talwalkar, and Virginia Smith. 2020. Federated Optimization in Heterogeneous Networks. In *MLSys*. mlsys.org.
- [30] Ming-Yu Liu, Thomas M. Breuel, and Jan Kautz. 2017. Unsupervised Image-to-Image Translation Networks. In *NIPS*. 700–708.
- [31] Risheng Liu, Zi Li, Yuxi Zhang, Xin Fan, and Zhongxuan Luo. 2020. Bi-level Probabilistic Feature Learning for Deformable Image Registration. In *IJCAI*.
- [32] Brendan McMahan, Eider Moore, Daniel Ramage, Seth Hampson, and Blaise Agüera y Arcas. 2017. Communication-efficient learning of deep networks from decentralized data. In *Artificial intelligence and statistics*. PMLR, 1273–1282.
- [33] Brendan McMahan, Eider Moore, Daniel Ramage, Seth Hampson, and Blaise Agüera y Arcas. 2017. Communication-Efficient Learning of Deep Networks from Decentralized Data. In *AISTATS (Proceedings of Machine Learning Research, Vol. 54)*. PMLR, 1273–1282.
- [34] Tony C. W. Mok and Albert C. S. Chung. 2020. Fast Symmetric Diffeomorphic Image Registration with Convolutional Neural Networks. *2020 IEEE/CVF Conference on Computer Vision and Pattern Recognition (CVPR)* (2020), 4643–4652.
- [35] Xavier Pennec, Pascal Cachier, and Nicholas Ayache. 1999. Understanding the “demon’s algorithm”: 3D non-rigid registration by gradient descent. In *International Conference on Medical Image Computing and Computer-Assisted Intervention*. Springer, 597–605.
- [36] Mengwei Ren, Neel Dey, James Fishbaugh, and Guido Gerig. 2021. Segmentation-Renormalized Deep Feature Modulation for Unpaired Image Harmonization. *IEEE Transactions on Medical Imaging* 40, 6 (2021), 1519–1530.
- [37] Marc-Michel Rohé, Manasi Datar, Tobias Heimann, Maxime Sermesant, and Xavier Pennec. 2017. SVF-Net: Learning Deformable Image Registration Using Shape Matching. In *MICCAI*.
- [38] Olaf Ronneberger, Philipp Fischer, and Thomas Brox. 2015. U-Net: Convolutional Networks for Biomedical Image Segmentation. *ArXiv abs/1505.04597* (2015).
- [39] Daniel Rueckert, Luke I Sonoda, Carmel Hayes, Derek LG Hill, Martin O Leach, and David J Hawkes. 1999. Nonrigid registration using free-form deformations: application to breast MR images. *IEEE transactions on medical imaging* 18, 8 (1999), 712–721.
- [40] Anmol Sharma and G. Hamarneh. 2020. Missing MRI Pulse Sequence Synthesis Using Multi-Modal Generative Adversarial Network. *IEEE Transactions on Medical Imaging* 39 (2020), 1170–1183.
- [41] Dinggang Shen and Christos Davatzikos. 2002. HAMMER: hierarchical attribute matching mechanism for elastic registration. *IEEE transactions on medical imaging* 21, 11 (2002), 1421–1439.
- [42] Liye Shen, Wentao Zhu, Xiaosong Wang, Lei Xing, John M. Pauly, Baris Turkbey, Stephanie A. Harmon, Thomas Sanford, Sherif Mehrhivand, Peter L. Choyke, Bradford J. Wood, and Daguang Xu. 2021. Multi-Domain Image Completion for Random Missing Input Data. *IEEE Transactions on Medical Imaging* 40 (2021), 1113–1122.
- [43] Rebecca L. Siegel, Kimberly D Miller, and Ahmedin Jemal. 2019. Cancer statistics, 2019. *CA: A Cancer Journal for Clinicians* 69 (2019).
- [44] Joonyoung Song and Jong Chul Ye. 2021. Federated CycleGAN for Privacy-Preserving Image-to-Image Translation. *CoRR abs/2106.09246* (2021).

- [45] J-P Thirion. 1998. Image matching as a diffusion process: an analogy with Maxwell's demons. *Medical image analysis* 2, 3 (1998), 243–260.
- [46] Alexander Thorley, Xi Jia, Hyung Jin Chang, Boyang Liu, Karina V Bunting, Victoria M. Stoll, Antonio de Marvao, Declan P. O'Regan, Georgios V. Gkoutos, Dipak Kotecha, and Jinming Duan. 2021. Nesterov Accelerated ADMM for Fast Diffeomorphic Image Registration. In *MICCAI*.
- [47] Hongyi Wang, Mikhail Yurochkin, Yuekai Sun, Dimitris S. Papailiopoulos, and Yasaman Khazaeni. 2020. Federated Learning with Matched Averaging. In *ICLR*. OpenReview.net.
- [48] Jian Wang and Miaomiao Zhang. 2020. DeepFLASH: An Efficient Network for Learning-Based Medical Image Registration. *2020 IEEE/CVF Conference on Computer Vision and Pattern Recognition (CVPR)* (2020), 4443–4451.
- [49] Yan Wang, Luping Zhou, Lei Wang, Biting Yu, Chen Zu, David S. Lalush, Weili Lin, Xi Wu, Jiliu Zhou, and Dinggang Shen. 2018. Locality Adaptive Multi-modality GANs for High-Quality PET Image Synthesis. *Medical image computing and computer-assisted intervention : MICCAI ... International Conference on Medical Image Computing and Computer-Assisted Intervention* 11070 (2018), 329–337.
- [50] Guoyang Xie, Jinbao Wang, Yawen Huang, Yuexiang Li, Yefeng Zheng, Feng Zheng, and Yaochu Jin. 2022. FedMed-GAN: Federated Domain Translation on Unsupervised Cross-Modality Brain Image Synthesis.
- [51] Jing Yang, Yinghao Wu, Dong Zhang, Wenting Cui, Xiaoli Yue, S. Du, and Hongmei Zhang. 2022. LDVoxelMorph: A precise loss function and cascaded architecture for unsupervised diffeomorphic large displacement registration. *Medical physics* (2022).
- [52] Biting Yu, Luping Zhou, Lei Wang, Jurgen Fripp, and Pierrick T. Bourgeat. 2018. 3D cGAN based cross-modality MR image synthesis for brain tumor segmentation. *2018 IEEE 15th International Symposium on Biomedical Imaging (ISBI 2018)* (2018), 626–630.
- [53] Biting Yu, Luping Zhou, Lei Wang, Yinghuan Shi, Jurgen Fripp, and Pierrick T. Bourgeat. 2020. Sample-Adaptive GANs: Linking Global and Local Mappings for Cross-Modality MR Image Synthesis. *IEEE Transactions on Medical Imaging* 39 (2020), 2339–2350.
- [54] Mikhail Yurochkin, Mayank Agarwal, Soumya Ghosh, Kristjan H. Greenewald, Trong Nghia Hoang, and Yasaman Khazaeni. 2019. Bayesian Nonparametric Federated Learning of Neural Networks. In *ICML (Proceedings of Machine Learning Research, Vol. 97)*. PMLR, 7252–7261.
- [55] Bo Zhou, Chi Liu, and James S. Duncan. 2021. Anatomy-Constrained Contrastive Learning for Synthetic Segmentation without Ground-truth. In *MICCAI*.
- [56] Jun-Yan Zhu, Taesung Park, Phillip Isola, and Alexei A Efros. 2017. Unpaired image-to-image translation using cycle-consistent adversarial networks. In *Proceedings of the IEEE international conference on computer vision*. 2223–2232.
- [57] Qing Zuo, Jianping Zhang, and Yin Yang. 2021. DMC-Fusion: Deep Multi-Cascade Fusion With Classifier-Based Feature Synthesis for Medical Multi-Modal Images. *IEEE Journal of Biomedical and Health Informatics* 25 (2021), 3438–3449.